Modeling *Plasmodium falciparum* Diagnostic Test Sensitivity using Machine Learning with Histidine-Rich Protein 2 Variants

Colby T Ford [1,2,*], **Gezahegn Alemayehu** [3], **Kayla Blackburn** [4], **Karen Lopez** [1], **Cheikh Cambel Dieng** [4], **Lemu Golassa** [3], **Eugenia Lo** [4], **and Daniel Janies** [1]

[1] *Department of Bioinformatics and Genomics, University of North Carolina at Charlotte, Charlotte, NC USA*

[2] *School of Data Science, University of North Carolina at Charlotte, Charlotte, NC USA*

[3] *Aklilu Lemma Institute of Pathobiology, Addis Ababa University, Addis Ababa, Ethiopia*

[4] *Department of Biological Sciences, University of North Carolina at Charlotte, Charlotte, NC USA*

Correspondence*:
Corresponding Author
colby.ford@uncc.edu

ABSTRACT

Malaria, predominantly caused by *Plasmodium falciparum*, poses one of largest and most durable health threats in the world. Previously, simplistic regression-based models have been created to characterize malaria rapid diagnostic test performance, though these models often only include a couple genetic factors. Specifically, the Baker et al., 2005 model uses two types of particular repeats in histidine-rich protein 2 (PfHRP2) to describe a *P. falciparum* infection (Baker et al., 2005), though the efficacy of this model has waned over recent years due to genetic mutations in the parasite.

In this work, we use a dataset of 100 *P. falciparum* PfHRP2 genetic sequences collected in Ethiopia and derived a larger set of motif repeat matches for use in generating a series of diagnostic machine learning models. Here we show that the usage of additional and different motif repeats in more sophisticated machine learning methods proves effective in characterizing PfHRP2 diversity. Furthermore, we use machine learning model explainability methods to highlight which of the repeat types are most important with regards to rapid diagnostic test sensitivity, thereby showcasing a novel methodology for identifying potential targets for future versions of rapid diagnostic tests.

Keywords: Malaria, *Plasmodium falciparum*, Rapid Diagnostic Test, Machine Learning, Model Explainability

1 INTRODUCTION

There are over 228 million infections of malaria yearly and, in 2018, resulted in 405,000 deaths (World Health Organization, 2020). Genomics is beginning to bear fruit in abatement of malaria but presents

21 analytical challenges due to the complexity of the disease and its components (human, *Plasmodium spp.*,
22 and vector mosquitoes).

23 In most developing countries, the detection of *Plasmodium falciparum* and diagnosis of malaria is often
24 performed using simple rapid diagnostic tests (RDTs). Specifically, these tests are lateral flow immuno-
25 chromatographic antigen detection tests that are similar in modality to common at-home pregnancy tests.
26 These tests use dye-labeled antibodies to bind to a particular parasite antigen and display a line on a test
27 strip if the antibodies bind to the antigen of interest (WHO, 2015). In many parts of Africa, RDTs are
28 designed to detect the presence of *P. falciparum*'s histidine-rich protein 2 (PfHRP2). In fact, PfHRP2-based
29 RDTs accounted for around 74% of all RDTs used in sub-Saharan Africa in 2016 (WHO, 2016).

30 If patients are properly diagnosed, *P. falciparum* infections may be treated using antimalarial drugs
31 such as artemisinin or artemisinin combined therapies (ACTs). Unfortunately, the efficacy of RDTs and
32 artemisinin treatment have diminished in some settings around world, specifically in locations where the
33 deletion or mutation of the kelch domain–carrying protein *K13* gene are observed as is the case in Ethiopia
34 (Ouattara et al., 2015).

35 In 2005, Baker et al. published a simple linear regression-based model that purports to predict the
36 detection sensitivity of RDTs using a small fraction of genetic sequence variants that code for PfHRP2
37 (Baker et al., 2005). While with the data available at the time, the accuracy of the Baker model was high
38 (87.5%), the explanation ability of the RDT sensitivity was low (R^2 = 0.353). Enthusiasm for the Baker
39 model has since diminished. In 2010, Baker et al. published a report in which they concluded that they can
40 no longer correlate sequence variation and RDT failure with their model (Baker et al., 2010). Nevertheless,
41 there is no alternative to the Baker model and it is still in use.

42 Given that simple correlation fails to show definitive relationships between motif repeats and RDT results,
43 we looked to machine learning as a more advanced alternative. In this study, our hypothesis is that a model
44 for understanding the relationship between RDT test sensitivity and sequence variation can be improved by
45 using a larger set of genetic sequence variants with better machine learning modeling. Our purpose is to
46 use molecular datasets and machine learning methods to address the shortcomings in malaria diagnosis test
47 sensitivity[1] and to provide a novel approach to direct the development of future RDTs using PfHRP2. In
48 this study, we analyze a collection of genetic data and metadata from 100 *P. falciparum* sequences collected
49 from Ethiopia with the Baker model along with a sweep of other machine learning models that we generate.

50 Beyond simply training a better model using more sophisticated algorithms, our research focus is to allow
51 for interpretable insights of the machine learning models to be derived from the "black box". We have
52 shown previous success in AI-driven explanations of gene expression underlying drug resistant strains of
53 *Plasmodium falciparum* (Davis et al., 2019; Ford and Janies, 2020). We apply this model interpretability
54 here to identify which types of histidine-rich repeats, present in PfHRP2, are most indicative of malaria
55 test performance.

56 While our work here only uses a relatively small dataset from a single African country, our purpose is to
57 showcase the utility of machine learning model interpretation for the improvement and design of future
58 RDTs.

---

[1] "Sensitivity" here refers to the ability of a RDT to detect a malaria infection despite genetic variations of the parasite. Elsewhere in this article in relation to machine learning, this term is used to describe the statistical measure also known as "true positive rate".

---

2 MATERIALS AND METHODS

2.1 Data Collection

Blood samples and demographic data were collected from suspected malaria patients greater than five years of age in various health clinics during both the low and high transmission seasons in different regions of Assosa, Ethiopia. Specifically, this health facility-based, cross-sectional study was conducted in febrile patients seeking malaria diagnosis at four selected health facilities: Assosa, Bambasi, Kurmuk and Sherkole from November to December 2018. *Note: This work encompasses the same set of samples as described in Alemayehu et al. (2020).*

Microscopy and rapid diagnostic testing were performed within the health clinics, and drops of blood spotted on Whatman 3MM filter paper were kept in sealed pouches for later analyses. CareStart™ malaria combination RDTs (lot code 18H61 from Access Bio Ethiopia) were used to diagnose *P. falciparum* and to evaluate their performance against microscopy as a reference test.
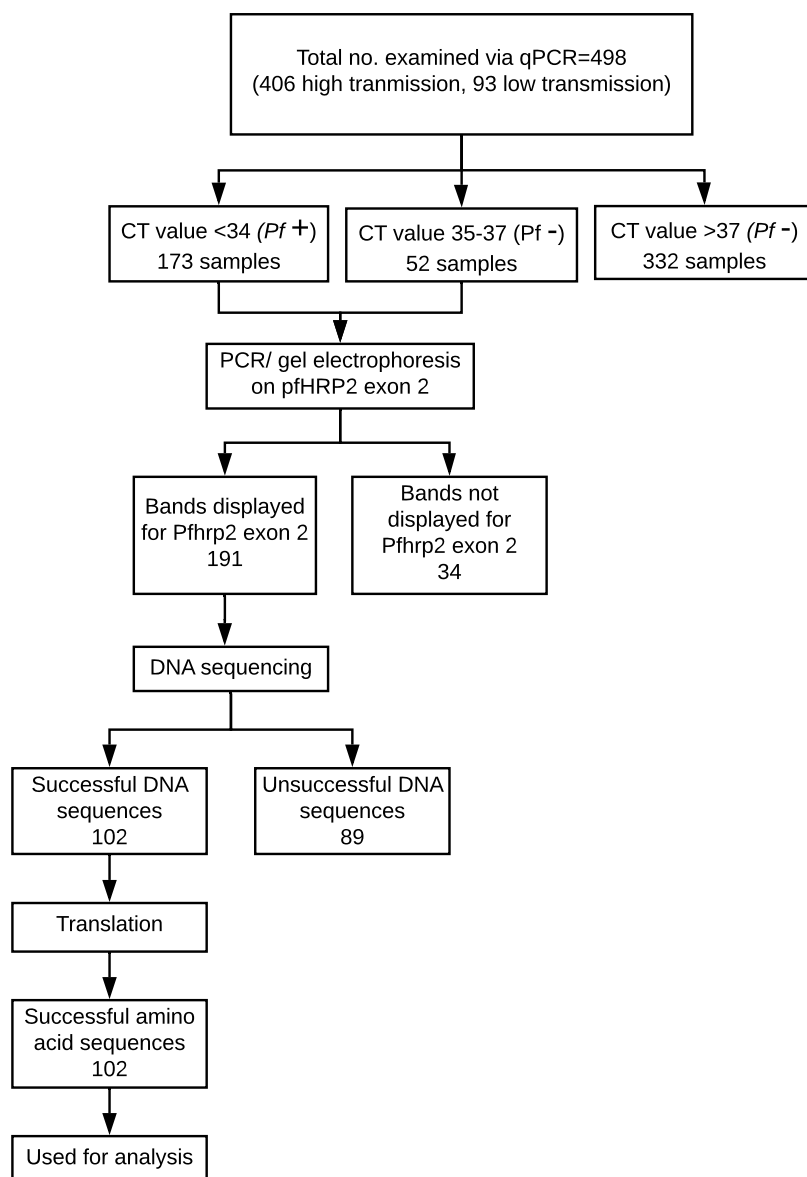
The *P. falciparum* DNA concentration in dried blood spot samples was analyzed using real-time quantitative PCR (RT-PCR). The *P. falciparum* DNA was extracted using phosphate buffered saline, Saponin, and Chelex (R.B. et al., 2013) and confirmed *P. falciparum* positive samples as those whose RT-PCR values were less than or equal to 37 (G. et al., 1993). The null hypothesis was that RDT testing and the detection of *P. falciparum* by RT-PCR will have a strong correlation (e.g., positive RDT samples will lead to positive RT-PCR and negative RDT samples will lead to negative RT-PCR). However, early findings have shown incongruence between the RDT results and RT-PCR (Alemayehu et al., 2020).

Using the primers listed in Table 3, two amplicons were sequenced, including a 600 to 960-bp fragment for Pfhrp2 Exon 2 (Baker et al., 2005) and a 294 to 552-bp fragment for Pfhrp3 Exon 2 (Baker et al., 2010). Each sample was sequenced once, in both forward and reverse directions to create a consensus sequence for each sample. Polymerase Chain Reaction (PCR) conditions for Pfhrp2 Exon 2 and Pfhrp3 Exon 2 are also shown in Table 3. The DNA amplicon quality was observed by means of agarose gel electrophoresis and the bands visualized in a UV transilluminator. PCR products were cleaned with 10 units of Exonuclease I (Thermo Scientific) and 0.5 units of shrimp alkaline phosphatase (Affymetrix) at 37 °C for 1 h followed by a 15 min incubation at 65 °C to deactivate the enzymes. PCR products were sequenced with ABI BigDye Terminator v3.1 (Thermo Fisher Scientific) following the manufacturer's protocol using the conditions of (1) 95 °C for 10 s, (2) 95 °C for 10 s, (3) 51 °C for 5 s, (4) 60 °C for 4 min, and (5) repeat steps 2-4 for 39 more cycles. The samples were cleaned using Sephadex G-50 (Sigma-Aldrich) medium in a filter plate and centrifuged in a vacufuge to decant.

The samples were reconstituted with Hi-Di Formamide (Thermo Fisher Scientific) and the plates were placed on the ABI 3130 Sequencer. Sequence trace files from all samples and repeat samples were imported into CodonCode Aligner (CodonCode Corporation). The bases were called for each sample. The ends of the sequences were trimmed by the application when possible and manually when necessary. All sequences were examined and evaluated on both the forward and reverse strands, with manual base corrections and manual base calls occurring when necessary. This resulted in 102 usable sequences, of which 100 had a corresponding and conclusive RDT and qPCR results.

2.2 Data Preparation

All Pfhrp2 exon 2 nucleotide sequences were exported from CodonCode Aligner (CodonCode Corporation) and individually pasted into the ExPASy Translate tool (Swiss Institute of Bioinformatics Resource Portal). Both forward and reverse DNA strands were translated using the standard NCBI genetic code. The six reading frames of the amino acid sequence produced were examined. CodonCode's default

Total no. examined via qPCR=498
(406 high tranmission, 93 low transmission)

CT value <34 (*Pf* +)
173 samples

CT value 35-37 (Pf -)
52 samples

CT value >37 (*Pf* -)
332 samples

PCR/ gel electrophoresis
on pfHRP2 exon 2

Bands displayed
for Pfhrp2 exon 2
191

Bands not
displayed for
Pfhrp2 exon 2
34

DNA sequencing

Successful DNA
sequences
102

Unsuccessful DNA
sequences
89

Translation

Successful amino
acid sequences
102

Used for analysis

Figure 1. Breakdown of *P. falciparum* samples used in this study. 100 of the final 102 sequences have corresponding and conclusive RDT and qPCR results and thus were used in the machine learning analysis.

		qPCR Result		Totals
		+ (id: 1)	- (id: 2)	
RDT Result	+ (id: 1)	62 True Positives	4 False Positives	66 Total RDT Positives
	- (id: 2)	12 False Negatives	22 True Negatives	34 Total RDT Negatives
Totals	Totals	74 Total qPCR Positives	26 Total qPCR Negatives	100 Total Conclusive Results

Table 1. Confusion matrix of conclusive RDT results versus qPCR results.

101 parameters were used for clipping the ends and a visual check was performed of each sequence to ensure
102 base calls were correct, and trimmed further as needed.

Statistic	(%)
Accuracy	84.0%
Sensitivity (True Positive Rate)	83.8%
Specificity (True Negative Rate)	84.6%
F_1 Score	88.6%

Table 2. Derived statistics from Table 1 with regards to RDT performance compared to qPCR validation. Note that the term "sensitivity" here refers to the statistical measure of the true positive rate.
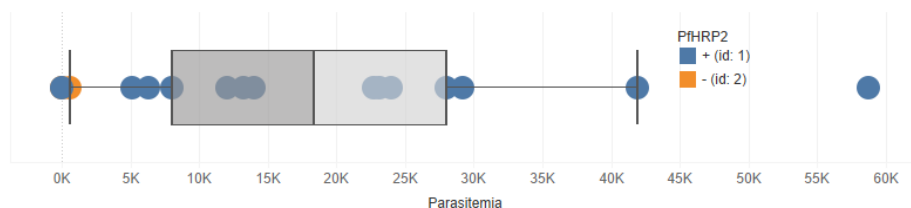
Figure 2. Boxplot showing the distribution of parasitemia among the 100 samples used in this study. Blue points represent RDT-positive cases and orange points represent RDT-negative cases. Note that there are some RDT-positive samples that with zero parasitemia.

Gene	Primer	Direction	Sequence '5——3'	PCR Program
Pfhrp2 Exon2	pfhrp2_ex2_F_Parr	Forward	ATTCCGCATTTAATAATAACTTGTGTAGC	95°C×15 min; 40 cycles of 94°C×1 min
	pfhrp2_ex2_R_Parr	Reverse	ATGGCGTAGGCAATGTGTGG	59°C×1 min, 72°C×1 min; 72°C×10 min

Table 3. PCR Conditions and Primer Sequences from Parr et al., 2018 (Parr et al., 2018).

103   For each nucleotide sequence, the amino acid sequence presenting the fewest number of stop codons
104 was selected for further analysis. If two or more of the reading frames appeared to produce sequences
105 with an equally minimal number of stop codons, the reading frame that produced a sequence exhibiting
106 the previously recognized pattern in prior sequences was selected for further analysis. While most of the
107 sequences had a clear, single best translation, 11 of the sequences required further editing. In these 11
108 sequences, the sequence portion before or after the stop codon which exhibited a pattern similar to prior
109 sequences was used in analysis, while the portion of the sequence preceding or following the stop codon,
110 which did not exhibit the recognized pattern, was discarded. Nucleotide sequence input into the ExPASy
111 Translate Tool (Swiss Institute of Bioinformatics Resource Portal) was repeated and verified for accuracy
112 of amino acid sequences. The verified sequences were compiled.

113   This process resulted in a final dataset of 74 PCR-positive samples, of which 12 (16%) were RDT-negative
114 and 62 (84%) were RDT-positive.

115 2.2.1   Motif Search

116   A motif search was performed across 24 different types of histidine-based repeats. These repeat types,
117 listed in Table 5, were originally defined by Baker et al. (2010). This search was completed using the
118 `motif.find()` function in the *bio3d* package in R (B.J. et al., 2006). Specifically, each amino acid
119 sequence was searched for each of the 24 repeat motifs and the count of matches was reported back into
120 the data. See Table 4. The breakdown of match frequencies by location is shown in Figure 4.

121 **2.3   Machine Learning**

122   In this work, three machine learning experiments were created on different sets of features: 1.) using
123 only the types that are in the original Baker model (Types 2 and 7), 2.) using all motif repeat type counts

124 (Types 1 through 24), and 3.) using only the features found to be important in the experiment with all motif
125 repeat types (Types 3, 5, and 10). Note that the *PfHRP2* column in Table 4 is treated as the dependent
126 variable in which a "1" represents a positive RDT result for malaria and a "2" represents a negative RDT
127 result. The motif repeat types are used as the independent variables and the *PfHRP2* column is treated as
128 the dependent variable.

129 We used the Microsoft Azure Machine Learning Service (Microsoft, 2019c) as the tracking platform for
130 retaining model performance metrics as the various models were generated. For this use case, multiple
131 machine learning models were trained using various scaling techniques and algorithms. Scaling and
132 normalization methods are shown in Table 7. We then created two ensemble models of the individual
133 models using stack ensemble and voting ensemble methods.

134 The Microsoft AutoML package (Microsoft, 2019a) allows for the parallel creation and testing of various
135 models, fitting based on a primary metric. For this use case, models were trained using Decision Tree,
136 Elastic Net, Extreme Random Tree, Gradient Boosting, Lasso Lars, LightGBM, RandomForest, and
137 Stochastic Gradient Decent algorithms along with various scaling methods from Maximum Absolute

id	dna_sequence	aa_sequence	Type_1	Type_2	…	Type_24	PfHRP2
HAss14	AATAAGAGAT…	NKRLLHETQA…	9	9	…	0	1
HAss42	ATAAGAGATT…	KRLLHETQAH…	0	0	…	0	2
…	…	…	…	…	…	…	…
LShr5	TATTACACGA…	LHETQAHVDD…	0	0	…	0	1

Table 4. Example data format with counts of Types 1 through 24 matches in the amino acid sequence. In the PfHRP2 column, a "1" represents positive cases and a "2" represents negative cases of malaria.

Type	Sequence	PfHRP2	PfHRP3
1	AHHAHHVAD	+	+
2	AHHAHHAAD	+	+
3	AHHAHHAAY	+	-
4	AHH	+	+
5	AHHAHHASD	+	-
6	AHHATD	+	-
7	AHHAAD	+	+
8	AHHAAY	+	-
9	AAY	+	-
10	AHHAAAHHATD	+	-
11	AHN	+	-
12	AHHAAAHHEAATH	+	-
13	AHHASD	+	-
14	AHHAHHATD	+	-
15	AHHAHHAAN	-	+
16	AHHAAN	-	+
17	AHHDG	-	+
18	AHHDD	-	+
19	AHHAA	+	-
20	SHHDD	+	+
21	AHHAHHATY	+	-
22	AHHAHHAGD	+	-
23	ARHAAD	+	-
24	AHHTHHAAD	+	-

Table 5. PfHRP2 and PFHRP3 repeat motif types as defined by Baker et al. (2010).

138 Scaler, Min/Max Scaler, Principal Component Analysis, Robust Scaler, Sparse Normalizer, Standard Scale
139 Wrapper, Truncated Singular Value Decomposition Wrapper (as defined in Table 7). All of the machine
140 learning algorithms are from the *scikit-learn* package (Pedregosa et al., 2011) except for LightGBM, which
141 is from the *LightGBM* package (Ke et al., 2017). The settings for the model sweep are defined in Table 6.
142 The Monte Carlo cross validation by default takes 10% of the initial training data set as the validation set.
143 The validation set is then used for metrics calculation.

Parameter	Value
Task	Classification
Training Time (hours)	3
Primary Metric	Precision score weighted
Validation type	Monte Carlo cross validation

**Table 6.** Parameter settings for the model searches.

Scaling and Normalization	Description
StandardScaleWrapper	Standardize features by removing the mean and scaling to unit variance
MinMaxScalar	Transforms features by scaling each feature by that column's minimum and maximum
MaxAbsScaler	Scale each feature by its maximum absolute value
RobustScalar	This scales features by their quantile range
PCA	Linear dimensionality reduction using singular value decomposition of the data to project it to a lower dimensional space
TruncatedSVDWrapper	This transformer performs linear dimensionality reduction by means of truncated singular value decomposition. Contrary to PCA, this estimator does not center the data before computing the singular value decomposition. This means it can efficiently work with sparse matrices.
SparseNormalizer	Each sample (each record of the data) with at least one non-zero component is re-scaled independently of other samples so that its norm (L1 or L2) equals one

Table 7. Scaling function options in the machine learning model search Microsoft (2019b).

144 For the experiment using only Types 2 and 7, 35 models were trained. For the experiment using Types
145 1 through 24, 35 models were trained. For the experiments using Types 3, 5, and 10, 31 models were
146 trained. This variation in the number of models trained is a factor of the automated model and parameter
147 selection process. When an assumed optimal model and parameter set is found, the algorithm stops training
148 individual models and then performs ensembling of the various singular models that were trained.

149 Two ensemble models (voting ensemble and stack ensemble) were created and tested for each experiment.
150 The voting ensemble method makes a prediction based on the weighted average of the previous models'
151 predicted classification outputs whereas the stacking ensemble method combines the previous models and
152 trains a meta-model using the elastic net algorithm based on the output from the previous models. The
153 model selection method used was the Caruana ensemble selection algorithm (Caruana et al., 2004).
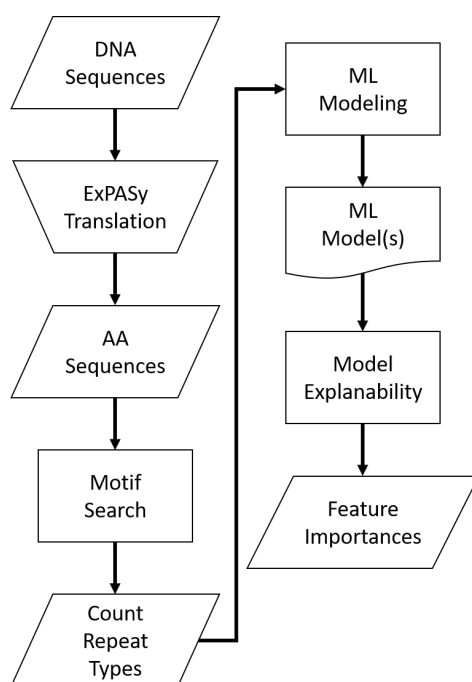
Figure 3. Analysis process flow.

2.4 Repeat Type Prevalence

As shown in Figure 4 and Table 8, many of the repeat types described by Baker et al. (2010) (Table 5) are represented in the Ethiopian sequences analyzed in this study. Specifically, Types 1-10, 12-14, and 19 were found among these isolates. This is in general agreement to a similar report by Willie et al. (2018) using samples collected from Papua New Guinea. They report that Types 1, 2, 6, 7, and 12 were present in almost all ($\geq 89\%$) sequences, Types 3, 5, 8, and 10 were present in most ($\geq 56\%$) sequences, and Type 4, 13, and 19 were seen in $\leq 33\%$ of sequences. In contrast, we see a higher prevalence of Types 4 and 19 and a lower prevalence of Type 12 than in the previous study.

Another study by Bharti et al. (2016) that used samples collected from multiple sites in India, reported that Types 1, 2, 7, and 12 were seen in 100% of their sequences. However, in our sequences from Ethiopia, we see multiple examples where these repeats are not present, especially Type 12.
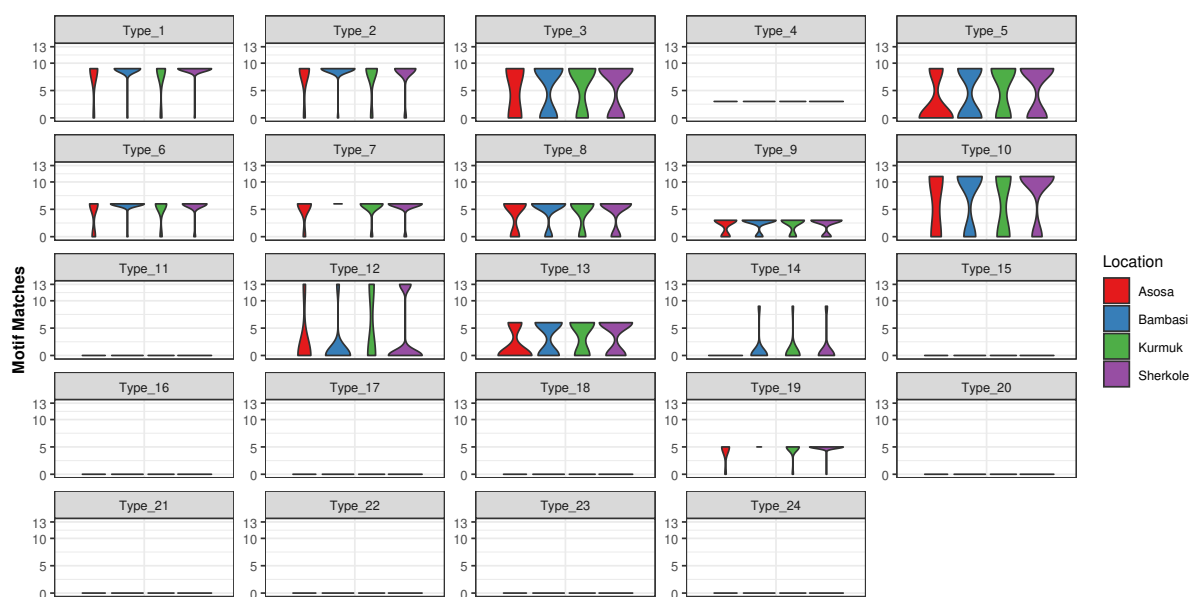
Figure 4. Type Frequencies by Location.

| Type	Asosa	Bambasi	Kurmuk	Sherkole	*Overall*
1	85.71%	97.06%	84.62%	97.92%	*95.10%*
2	85.71%	97.06%	84.62%	91.67%	*92.16%*
3	57.14%	61.76%	69.23%	66.67%	*64.71%*
4	100.00%	100.00%	100.00%	100.00%	*100.00%*
5	28.57%	50.00%	61.54%	62.50%	*55.88%*
6	71.43%	97.06%	84.62%	93.75%	*92.16%*
7	85.71%	100.00%	92.31%	93.75%	*95.10%*
8	71.43%	82.35%	76.92%	77.08%	*78.43%*
9	71.43%	82.35%	76.92%	77.08%	*78.43%*
10	57.14%	67.65%	53.85%	77.08%	*69.61%*
11	0.00%	0.00%	0.00%	0.00%	*0.00%*
12	14.29%	8.82%	38.46%	25.00%	*20.59%*
13	28.57%	55.88%	61.54%	62.50%	*57.84%*
14	0.00%	8.82%	7.69%	10.42%	*8.82%*
15	0.00%	0.00%	0.00%	0.00%	*0.00%*
16	0.00%	0.00%	0.00%	0.00%	*0.00%*
17	0.00%	0.00%	0.00%	0.00%	*0.00%*
18	0.00%	0.00%	0.00%	0.00%	*0.00%*
19	85.71%	100.00%	92.31%	97.92%	*97.06%*
20	0.00%	0.00%	0.00%	0.00%	*0.00%*
21	0.00%	0.00%	0.00%	0.00%	*0.00%*
22	0.00%	0.00%	0.00%	0.00%	*0.00%*
23	0.00%	0.00%	0.00%	0.00%	*0.00%*
24	0.00%	0.00%	0.00%	0.00%	*0.00%*

Table 8. Overall prevalence of each repeat type by location. Values represent the percentage of samples in which the repeat type was found.

3 RESULTS

165 Metrics from the three experiments' machine learning models (one each for the best ensemble model and a
166 best singular model) are reported in Table 9. The precision-recall curves for these models are shown in
167 Table 11 and the receiver operating characteristic (ROC) curves are shown in Table 10. The ideal scenario
168 is shown as a dash-dot-dash (-··-) line. The best model overall is the Extreme Random Trees model using
169 only Types 3, 5, and 10. This was determined by looking at the overall model metrics and the generated
170 curves. Note that many models were generated for each experiment, some of which have equal overall
171 performance. The best ensemble model and most simplistic singular model are shown here, but all model
172 runs can be found in the Supplementary Data.

Types	Algorithm	Precision	Recall	Accuracy	AUC	F1
Types 2 and 7 Only	Voting Ensemble	0.73129	0.68571	0.68571	0.65833	0.64136
	Extreme Random Trees	0.73129	0.68571	0.68571	0.65833	0.64136
Types 1 through 24	Voting Ensemble	0.80245	0.82857	0.82857	0.62500	0.79982
	Extreme Random Trees	0.80245	0.82857	0.82857	0.61667	0.79982
Types 3, 5, and 10	Voting Ensemble	0.83816	0.85714	0.85714	0.70000	0.82839
	Extreme Random Trees	0.83816	0.85714	0.85714	0.70000	0.82839

Table 9. Model metrics for the best singular model and voting ensemble model for each experiment.
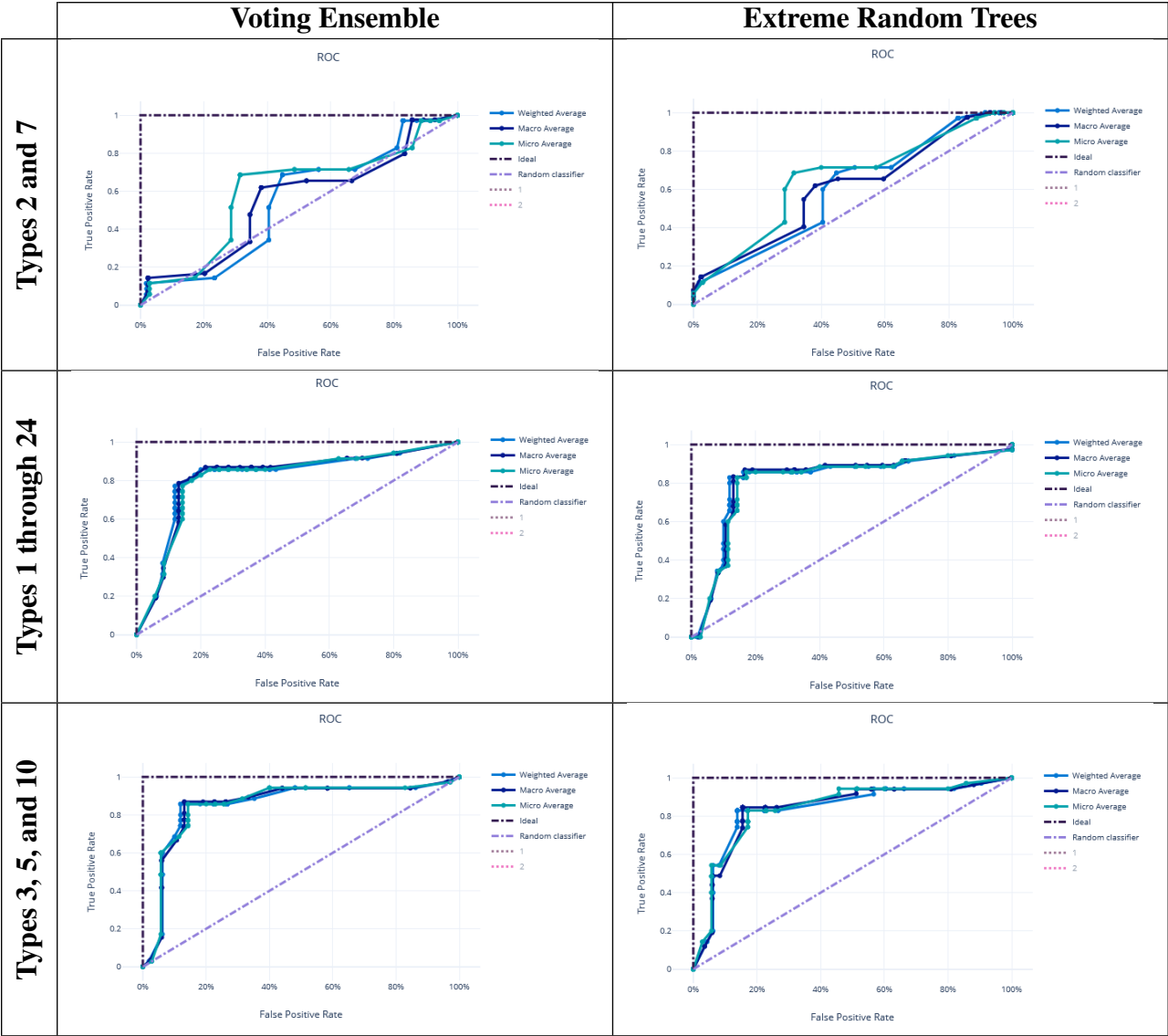
Table 10. ROC Curves for the best singular model and voting ensemble model for each experiment.
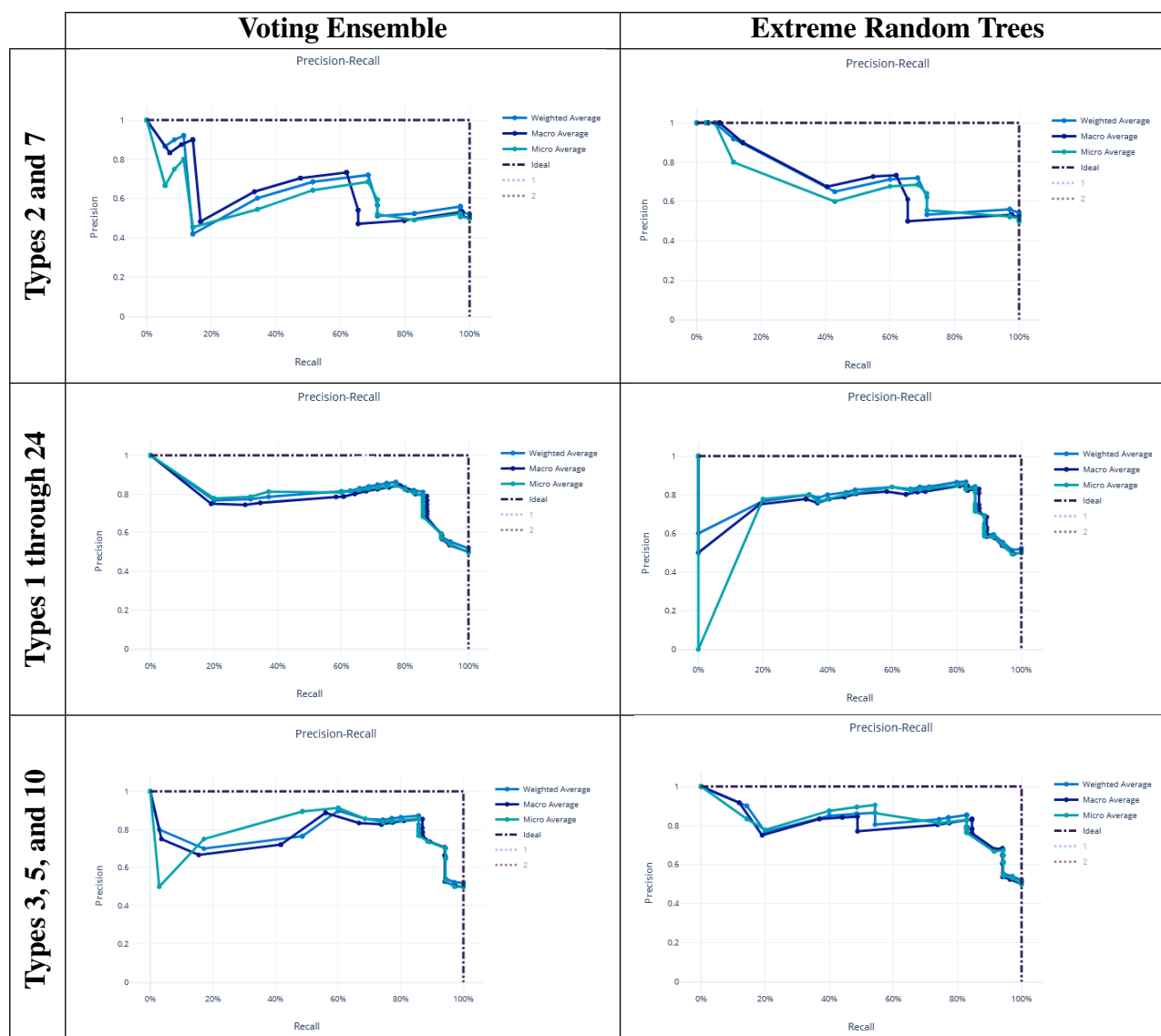
Table 11. Precision-Recall Curves for the best singular model and voting ensemble model for each experiment.
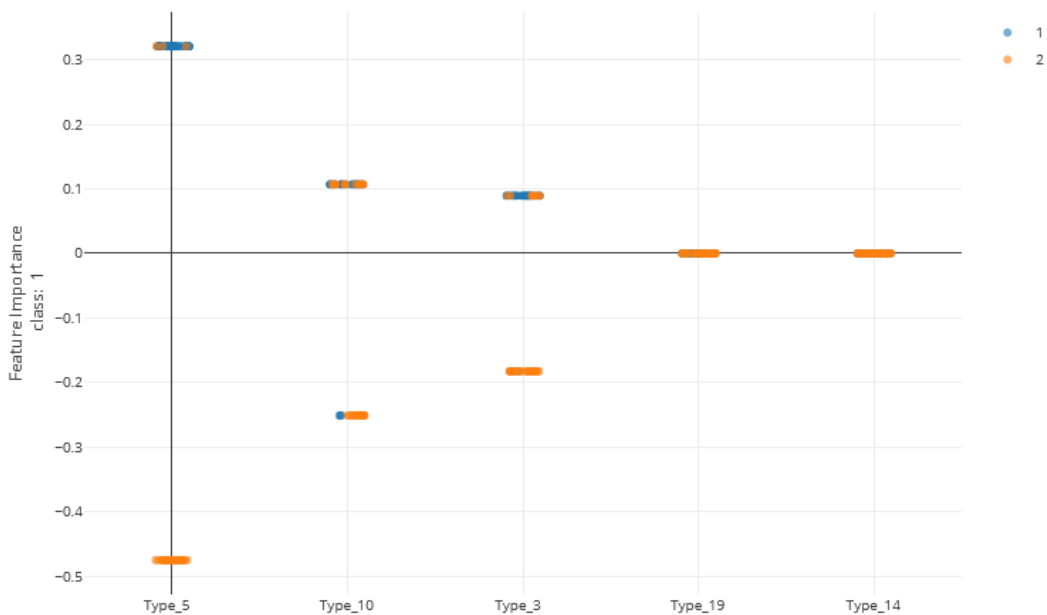
Feature importance

Feature importances were calculated using mimic-based model explanation of the voting ensemble model for Types 1 through 24. The mimic explainer works by training global surrogate models to mimic a black box model (Lundberg and Lee, 2017). The surrogate model is an interpretable model, trained to approximate the predictions of a black box model as accurately as possible (Molnar, 2019).

In the Voting Ensemble model using Types 1 through 24, Types 3, 5, and 10 were found to have non-zero importance. Types 3, 5, and 10 were then selected to train a more parsimonious model, which resulted in the best overall performance. See Figure 5.

	Global Importance	**Local Importance**
Type 3	0.15547	Min: -0.22644 Average: -4.14E-19 Std. Dev: 0.16433 Max: 0.22644
Type 5	0.48787	Min: -0.60532 Average: -1.66E-18 Std. Dev: 0.49919 Max: 0.60533
Type 10	0.28736	Min: -0.48132 Average: -2.49E-18 Std. Dev: 0.31516 Max: 0.48132

Table 12. Global and local feature importances of all features with non-zero importance (Types 3, 5, and 10) from the Voting Ensemble model using Types 1 through 24.

Figure 5. Local feature importance of the top 5 features. Note that only the top 3 have non-zero importances from the Voting Ensemble model using Types 1 through 24. Class "1" (orange dots) represents positive cases and class "2" (blue dots) represents negative cases of malaria.

4 DISCUSSION

181 Our work here is not to replace PCR-based testing, which is still reliable and accurate, but to use machine
182 learning to propose specific updates to RDTs. Given that RDTs are useful in remote settings and are
183 quicker and cheaper than PCR-based tests, their accuracy is crucial in the diagnosis of malaria and in the
184 epidemiological understanding of the spread of the disease.

185   Furthermore, our claim here is not that this preliminary machine learning model should be used across the
186 globe or even in Ethiopia without further validation. Instead, we are proposing that the derivation of feature
187 importance from ensembled machine learning models may prove beneficial in the understanding of RDT
188 sensitivity as a factor of complex polymorphic variations of genes. A limitation of this study is that only
189 100 samples were used from 4 locations in Ethiopia and this study only asserts the utility of RDTs based on
190 a single gene (Pfhrp2). This does not assess RDT sensitivity for other *P. falciparum* genes, isolates without

the Pfhrp2 gene (gene deletion), or the cross-reactivity of RDTs against the Pfhrp3 gene. Thus, there is a need to use larger datasets to increase our confidence in any machine learning model that is created and to sufficiently validate any model's findings with additional data from a similar parasite population.

Here we show the utility of machine learning in the identification of important factors in malaria diagnosis. Previous modeling by Baker et al. (2005) had shown that the parasitic infection can be diagnosed by looking at the prevalence of particular types of amino acid repeats. The original regression-based model may no longer by valid for this region of Ethiopia and, in this study, we show that even modeling Types 2 and 7 using more sophisticated machine learning algorithms fails to produce a reliable model of sensitivity. However, the usage of all Types 1 through 24 proves to make effective models that better characterize test performance to detect *P. falciparum* infections in our dataset. Furthermore, the usage of machine learning model explainability helps to pinpoint particular features of interest. In this case, Types 3, 5 and 10 reveal better diagnostic sensitivity for these malaria isolates collected from regions of Ethiopia.

Several studies have indicated that the Type 2 repeat (AHHAHHAAD) and Type 7 repeat (AHHAAD) have been described as possible epitopes targeted by monoclonal antibodies used to detect PfHRP2 (Baker et al., 2010; Lee et al., 2012). The highest frequency Types 2, 4, and 7 are also observed in some African countries (Deme et al., 2014). This is in agreement with our findings in this work for the Types that have a high prevalence frequency (between 85%-100%). However, our analysis here may reveal better diagnostic sensitivity for Types 3, 5, and 10, which have lower frequencies (between ~28%-70%) among the malaria isolates collected from our study area in Ethiopia. These Type prevalences by region are shown in Table 8.

When comparing the prevalences of Types in our Ethiopian samples (as shown in Table 8) to samples in other HRP2/3-based studies from other regions, there are often many differences in the breakdown of Types. For example, in the Type prevalences across the Indian samples in Kumar Bharti et al. (2017) (see Supplementary Data), we see that Types 2, 6, 7, and 12 are almost always seen and that the Types that are less pervasive (which seem to be important in understanding RDT sensitivity) vary drastically from the Ethiopian samples used in our study. Interestingly, in samples from a Papua New Guinea study by Willie et al. (2018), we see that Types 2, 7, and 12 are almost always seen and that Types are 3, 5, and 10 are less prevalent, similar to the findings in this study.

These comparisons support the argument that regional models must be created as a "one size fits all" approach to modeling RDT sensitivity will not be adequate given the global variability in the parasite. While some Types are quite common globally, the key to RDT sensitivity may lie in the Types that are less ubiquitous, as is shown in our study and is exemplified by the waning utility of Types 2 and 7 despite their common prevalence.

In future work, additional genetic factors need to be taken into account so that isolates without PfHRP2/3 are detected as well. It has been shown that a substantial portion of Ethiopian isolates experience PfHRP2 deletion in some regions (for example, over 62% of isolates in Eritrea) and, as such, this necessitates the evaluation of other genes when designing RDTs (Golassa et al., 2020). RDTs will only be able to test for a finite set of features, so we should ensure any modeling is performed on data that represents the entire diversity in a given region. This activity should be performed at a regional or smaller level as worldwide parasite diversity will be infeasible to capture in a small enough set of features that can be implemented in a single RDT. Our purpose here is to showcase this innovative methodology for highlighting such features in genetic data. Furthermore, we show an example insight that Types 3, 5, and 10 could be used in future RDTs upon further *in vitro* testing and validation.

5 CONCLUSION

In this work, we show the utility of employing broad machine learning modeling on various genetic features and then deriving the important features from top performing models to hone in on potential targets for future RDTs. This work posits the idea that RDTs can be revised to accommodate the genetic differences seen in today's *P. falciparum* infections and malaria cases. While this study focuses on a small region of Ethiopia, we can conclude that HRP2 variants may not correlate with RDT accuracy at a global level. Future versions of RDTs may be improved using our novel methodology for identifying genetic variants of interest to improve test sensitivity on a regional level. Though more work is to be done to empirically validate these findings, this *in silico* simulation may direct where to take experimental testing next. Also, while this work showcases important histidine-rich repeats of Types 3, 5, and 10, this is specific to the Ethiopian sequences used in this study and other *P. falciparum* strains in other regions may result in different results. Furthermore, training machine learning models on sets of malaria sequences from other areas such as Papua New Guinea, India, or other areas of Africa may reveal that different repeats are important in those areas, likely suggesting the RDTs may need to be region-specific due to variations in *P. falciparum* across the globe.

CONFLICT OF INTEREST STATEMENT

The authors declare that the research was conducted in the absence of any commercial or financial relationships that could be construed as a potential conflict of interest.

AUTHOR CONTRIBUTIONS

G.A. and L.G. designed and performed the patient recruitment and sampling. G.A, L.G. and D.J. managed ethical approval, funding, and visas. G.A., K.L., K.B., and C.C.D performed the DNA extractions, RT-PCR, PCR, and sequencing of the samples under the direction of L.G., D.J., and E.L. K.B. and D.J. performed the DNA to amino acid translations. C.T.F. performed the motif search for repeat types and performed all the machine learning and model interpretability work. All authors reviewed this manuscript.

FUNDING

DATA AVAILABILITY STATEMENT

All data, scripts, and model outputs are hosted on GitHub at: github.com/colbyford/pfHRP_MLModel

REFERENCES

Alemayehu, G. S., Lopez, K., Dieng, C. C., Lo, E., Janies, D., and Golassa, L. (2020). Evaluation of pfhrp2 and pfldh malaria rapid diagnostic test performance in assosa zone, ethiopia. *The American Journal of Tropical Medicine and Hygiene* 103, 1902–1909. doi:https://doi.org/10.4269/ajtmh.20-0485

Baker, J., Ho, M.-F., Pelecanos, A., Gatton, M., Chen, N., Abdullah, S., et al. (2010). Global sequence variation in the histidine-rich proteins 2 and 3 of plasmodium falciparum: implications for the performance of malaria rapid diagnostic tests. *Malaria Journal* 9, 129. doi:10.1186/1475-2875-9-129

Baker, J., McCarthy, J., Gatton, M., Kyle, D. E., Belizario, V., Luchavez, J., et al. (2005). Genetic Diversity of Plasmodium falciparum Histidine-Rich Protein 2 (PfHRP2) and Its Effect on the Performance of PfHRP2-Based Rapid Diagnostic Tests. *The Journal of Infectious Diseases* 192, 870–877. doi:10.1086/432010

Bharti, P. K., Chandel, H. S., Ahmad, A., Krishna, S., Udhayakumar, V., and Singh, N. (2016). Prevalence of pfhrp2 and/or pfhrp3 gene deletion in plasmodium falciparum population in eight highly endemic states in india. *PLOS ONE* 11, 1–16. doi:10.1371/journal.pone.0157949

B.J., G., A.P.C., R., K.M., E., J.A., M., and L.S.D., C. (2006). Bio3d: An r package for the comparative analysis of protein structures. *Bioinformatics* 22, 2695–2696

Caruana, R., Niculescu-Mizil, A., Crew, G., and Ksikes, A. (2004). Ensemble selection from libraries of models. In *Proceedings of the Twenty-first International Conference on Machine Learning* (New York, NY, USA: ACM), ICML '04, 18–. doi:10.1145/1015330.1015432

Davis, S., Button-Simons, K., Bensellak, T., Ahsen, E. M., Checkley, L., Foster, G. J., et al. (2019). Leveraging crowdsourcing to accelerate global health solutions. *Nature Biotechnology* 37, 848–850. doi:10.1038/s41587-019-0180-5

Deme, A. B., Park, D. J., Bei, A. K., Sarr, O., Badiane, A. S., Gueye, P. E. H. O., et al. (2014). Analysis of pfhrp2 genetic diversity in senegal and implications for use of rapid diagnostic tests. *Malaria Journal* 13, 34. doi:10.1186/1475-2875-13-34

Ford, C. T. and Janies, D. (2020). Ensemble machine learning modeling for the prediction of artemisinin resistance in malaria. *F1000Research* 9. doi:10.12688/f1000research.21539.1

G., S., S., V., X.P., Z., W., J., L., P., do Rosario V.E., et al. (1993). High sensitivity of detection of human malaria parasites by the use of nested polymerase chain reaction. *Molecular and Biochemical Parasitology* 61, 315–320

Golassa, L., Messele, A., Amambua-Ngwa, A., and Swedberg, G. (2020). High prevalence and extended deletions in plasmodium falciparum hrp2/3 genomic loci in ethiopia. *PLOS ONE* 15, 1–11. doi:10.1371/journal.pone.0241807

Ke, G., Meng, Q., Finley, T., Wang, T., Chen, W., Ma, W., et al. (2017). Lightgbm: A highly efficient gradient boosting decision tree. In *Advances in Neural Information Processing Systems 30*, eds. I. Guyon, U. V. Luxburg, S. Bengio, H. Wallach, R. Fergus, S. Vishwanathan, and R. Garnett (Curran Associates, Inc.). 3146–3154

Kumar Bharti, P., Singh Chandel, H., Krishna, S., Nema, S., Ahmad, A., Udhayakumar, V., et al. (2017). Sequence variation in plasmodium falciparum histidine rich proteins 2 and 3 in indian isolates: Implications for malaria rapid diagnostic test performance. *Scientific Reports* 7, 1308. doi:10.1038/s41598-017-01506-9

Lee, N., Gatton, M. L., Pelecanos, A., Bubb, M., Gonzalez, I., Bell, D., et al. (2012). Identification of optimal epitopes for Plasmodium falciparum rapid diagnostic tests that target histidine-rich proteins 2 and 3. *J. Clin. Microbiol.* 50, 1397–1405

Lundberg, S. M. and Lee, S.-I. (2017). A unified approach to interpreting model predictions. In *Advances in Neural Information Processing Systems 30*, eds. I. Guyon, U. V. Luxburg, S. Bengio, H. Wallach, R. Fergus, S. Vishwanathan, and R. Garnett (Curran Associates, Inc.). 4765–4774

Microsoft (2019a). *Azure Machine Learning AutoML Core version 1.0.79*

[Dataset] Microsoft (2019b). Microsoft Azure Machine Learning - AutoML Preprocessing

[Dataset] Microsoft (2019c). Microsoft Azure Machine Learning Service

Molnar, C. (2019). *Interpretable Machine Learning*. https://christophm.github.io/interpretable-ml-book/

Ouattara, A., Kone, A., Adams, M., Fofana, B., Maiga, A. W., Hampton, S., et al. (2015). Polymorphisms in the k13-propeller gene in artemisinin-susceptible plasmodium falciparum parasites from bougoula-hameau and bandiagara, mali. *The American Journal of Tropical Medicine and Hygiene* 92, 1202–1206. doi:https://doi.org/10.4269/ajtmh.14-0605

Parr, J. B., Anderson, O., Juliano, J. J., and Meshnick, S. R. (2018). Streamlined, pcr-based testing for pfhrp2- and pfhrp3-negative plasmodium falciparum. *Malaria Journal* 17, 137. doi:10.1186/s12936-018-2287-4

Pedregosa, F., Varoquaux, G., Gramfort, A., Michel, V., Thirion, B., Grisel, O., et al. (2011). Scikit-learn: Machine learning in Python. *Journal of Machine Learning Research* 12, 2825–2830

R.B., M., R.J., C., F., S., and M.C., S.-M. (2013). Evaluation of three different dna extraction methods from blood samples collected in dried filter paper in plasmodium subpatent infections from the amazon region in brazil. *Revista do Instituto de Medicina Tropical de Sao Paulo* 55, 205–208. doi:10.1590/S0036-46652013000300012

[Dataset] WHO (2015). How malaria rdts work

[Dataset] WHO (2016). World malaria report

Willie, N., Zimmerman, P. A., and Mehlotra, R. K. (2018). Plasmodium falciparum histidine-rich protein 2 gene variation in a malaria-endemic area of papua new guinea. *The American Journal of Tropical Medicine and Hygiene* 99, 697–703. doi:https://doi.org/10.4269/ajtmh.18-0137

[Dataset] World Health Organization (2020). Fact sheet about malaria